

A HYDRODYNAMICAL MECHANISM FOR GENERATING ASTROPHYSICAL JETS

Xavier Hernández,¹ Pablo L. Rendón,² Rosa G. Rodríguez-Mota,² and A. Capella³

Received 2013 April 8; accepted 2013 October 11

RESUMEN

Se muestra que si en un disco de acreción clásico falla la aproximación de disco estrecho dentro de un cierto radio, se debe dar una transición de trayectorias keplerianas hacia trayectorias en caída radial. Se espera que esta transición ocurra al interior de un cierto radio crítico, siempre y cuando los perfiles de densidad superficial tengan una pendiente mayor que $\Sigma(R) \propto R^{-1/2}$. Las trayectorias de caída dan lugar a una concentración de materia hacia las regiones centrales, donde la mayor parte de la materia será tragada por el objeto central. Mostramos, a través de un análisis hidrodinámico perturbativo, que lo anterior tiene como resultado natural la formación de un par de chorros (jets) polares bien colimados. Se propone un primer tratamiento analítico del problema, y se muestra que es posible generar chorros astrofísicos a partir de mecanismos puramente hidrodinámicos. El mecanismo aquí descrito complementa las ideas existentes sobre el papel de los campos magnéticos, que muy probablemente dan lugar a la colimación a gran escala y a la estabilidad de los chorros.

ABSTRACT

Whenever in a classical accretion disk the thin disk approximation fails interior to a certain radius, a transition from Keplerian to radial infalling trajectories should occur. We show that this transition is actually expected to occur interior to a certain critical radius, provided surface density profiles are steeper than $\Sigma(R) \propto R^{-1/2}$, and further, that it probably corresponds to the observationally inferred phenomena of thick hot walls internally limiting the extent of many stellar accretion disks. Infalling trajectories will lead to the convergent focusing and concentration of matter towards the very central regions, most of which will simply be swallowed by the central object. We show through a perturbative hydrodynamical analysis, that this will naturally develop a well collimated pair of polar jets. A first analytic treatment of the problem described is given, proving the feasibility of purely hydrodynamical mechanisms for astrophysical jet generation.

Key Words: accretion, accretion disks — hydrodynamics — galaxies: jets — ISM: jets and outflows

1. INTRODUCTION

Astrophysical jets occur over a large range of astronomical scales, from the stellar Newtonian scales of HH objects (e.g., Reipurth & Bally 2001), to the relativistic cases of microquasars and gamma ray bursts (e.g., Mirabel & Rodríguez 1999; Mészáros 2002), and to the Mega-parsec extragalactic scales of AGN jets (e.g., Marscher et al. 2002). Although the processes of propagation and collimation appear to be relatively well understood in terms of the interplay between the hydrodynamics of the problem (Scheuer 1974) and magnetic

¹Instituto de Astronomía, Universidad Nacional Autónoma de México, Mexico.

²Centro de Ciencias Aplicadas y Desarrollo Tecnológico, Universidad Nacional Autónoma de México, Mexico.

³Instituto de Matemáticas, Universidad Nacional Autónoma de México, Mexico.

fields (e.g., Blandford 1990), the precise mechanism of jet generation remains as the most uncertain part of the scheme.

Existing jet generation mechanisms focus on the interaction between the rotating material in the inner regions of the accretion disk and the magnetic field of the central (rotating or otherwise) star, or perhaps an external magnetic field threading the disk. See for example Blandford & Payne (1982), Henriksen & Valls-Gabaud (1994), Meier, Koide, & Uchida (2001), Price, Pringle, & King (2003). Although generically successful, detailed comparisons with observations do not always yield consistent results, e.g., Ferreira, Dougados, & Cabrit (2006). Further, the details of relative orientation of stellar spin, accretion disk and magnetic field configurations have to be supplied in highly specific manners.

As an alternative, we explore the possibility of a hydrodynamical jet generation mechanism where magnetic fields play no rôle, but only the intrinsic hydrodynamical physics of the interplay between the accretion and the central star wholly determine the characteristics of the jet. The main obstacle to such a scheme is the presence of a centrifugal barrier associated with the angular momentum content of the material in the accretion disk. We show, however, that the thin disk approximation for accretion disks, which is equivalent to the assumption of quasi-circular orbits for the disk (e.g., Pringle 1981), is expected to break down internal to a certain critical radius, resulting in a transition to quasi-radial flow for the disk. Then, an analytic first order perturbation treatment serves to demonstrate the feasibility of purely hydrodynamical jets. We show also that many generic features of observed astrophysical jets across a wide range of scales can be naturally accounted for in the general model presented. The presence of magnetic fields in jet phenomena is evident empirically. However, it is not impossible that their main contribution to the problem could be restricted to the radiation of the jet material and to its long range collimation, with purely hydrodynamical physics playing a part in the actual jet generation mechanisms.

The problem of jet formation has been studied extensively in the context of classical hydrodynamics, most often regarding fluid-body interactions. The appearance of stable coaxial jets resulting from radially-symmetric velocity fields over thin fluid sheets has been established by, among others, Taylor (1960). The rôle played by both the magnitude and the direction of velocity in the formation of this type of jet is the subject of a theoretical study by Glauert (1956), where it is shown that at the point at which the jet forms, a large velocity gradient is observed and momentum flux is constant, with horizontal momentum being transformed into vertical momentum. Similar results were obtained by King & Needham (1994), who provide an asymptotic study of a jet formed by a vertical plate accelerating into a semi-infinite expanse of stationary fluid of finite depth with a free surface and a gravitational restoring force. It is found that as the fluid approaches the plate in a horizontal direction, a gradual rise in free-surface elevation occurs. Eventually, a thin region is reached where the vertical velocity dominates the horizontal velocity as a consequence of the fluid finding it more difficult to overcome the inertia it would meet by continuing its horizontal motion than by escaping vertically towards the low-pressure free surface. In essence, this same mechanism can allow for jet formation in the context of the problem we study here.

In § 2 we develop the criterion for transition to radial flow in a standard accretion disk. The perturbative solution to the resulting problem of a radially infalling disk is then developed in § 3. § 4 presents trajectories for particular cases of the solution obtained in the previous section, in dimensionless units. Finally, we give our conclusions in § 5.

2. THE TRANSITION TO RADIAL FLOW

We start from a standard thin accretion disk where material orbits on quasi-circular Keplerian orbits around a central star of mass M . Assuming axial symmetry and cylindrical coordinates, the total angular momentum of a ring at radius R of width ΔR will be:

$$L = 2\pi R^3 \Delta R \Sigma(R) \Omega(R), \quad (1)$$

where Σ and Ω are the surface density and orbital frequency profiles of the disk, respectively. If the breaking torque on a given ring of the disk, due to its exterior ring is denoted by $\tau(R)$, the total breaking torque on the ring at radius R will be:

$$\tau_B = \tau(R + \Delta R) - \tau(R). \quad (2)$$

The rate of change of the angular momentum of the ring in question can now be calculated as:

$$\dot{L} = \tau_B = \frac{d\tau}{dR}\Delta R. \quad (3)$$

If at any radius a substantial fraction of the angular momentum of the ring is lost through viscous torques over an orbital period, the assumption of quasi-circular orbits will break down, and the disk will make a transition to mostly radial orbits. This condition can be stated as:

$$\frac{L}{2\dot{L}} < \frac{2\pi}{\Omega}. \quad (4)$$

Substitution of equations (1) and (2) into the above yields:

$$R^3\Omega^2\Sigma < 2\left(\frac{d\tau}{dR}\right), \quad (5)$$

as the condition for the onset of radial flow in the disk.

We can now introduce a model for the torques in terms of the rate of shear and the effective viscosity ν (e.g., von Weizsäcker 1943; Pringle 1981) as:

$$\tau = 2\pi R^3\nu\Sigma\frac{d\Omega}{dR}. \quad (6)$$

Taking $\Omega^2 = GM/R^3$ to substitute the above equation into condition (5) gives

$$(GM)^{1/2}\Sigma < -6\pi\frac{d}{dR}\left(R^{1/2}\nu\Sigma\right). \quad (7)$$

To proceed further we can take for example, $\nu = \text{constant}$ and a model for the disk surface density profile of the form:

$$\Sigma = \Sigma_0\left(\frac{R}{R_0}\right)^{-n}, \quad (8)$$

of the type often used in models of accretion disks when fitted to observations (e.g., Hughes et al. 2009). Use of the two above forms for ν and $\Sigma(R)$ reduces condition(7) to:

$$6\pi\nu(n - 1/2) > (GMR)^{1/2}. \quad (9)$$

The above condition will always be met in any accretion disk with $n > 1/2$, interior to a transition radius R_T given by:

$$R_T = \frac{[6\pi\nu(n - 1/2)]^2}{GM}. \quad (10)$$

It is interesting that directly observed accretion disks have spectra which when modelled typically yield $n \sim 1$, in general $0 < n < 1.5$, e.g., Hartmann et al. (1998), Lada et al. (2006), Hughes et al. (2009). This leads one to expect the transition to radial flow to occur in many of the stellar accretion disks, interior to radii given by equation (10).

Finally, we can explore the consequences of introducing an α prescription (Shakura & Sunyaev 1973) into condition (9), $\nu = \alpha cH$, where c and H are respectively the sound speed and height of the disk, with α a dimensionless number, yielding the dimensionless condition:

$$\mathcal{M}\left(\frac{R}{H}\right) < 6\pi\alpha(n - 1/2), \quad (11)$$

where \mathcal{M} is the ratio of the Keplerian orbital velocity in the disk to the sound speed in the disk. Although the above condition is only valid for constant ν , it illustrates the equivalence between the assumption of quasi-circular orbits for the material in the disk, and the assumption that the disk is thin. We see that the breakdown of the assumption of quasi-circular orbits (condition 9), corresponds to the point where disk becomes fat.

Writing \mathcal{M} in astrophysical units as:

$$\mathcal{M} = 1.8 \left(\frac{200K}{T} \right)^{1/2} \left(\frac{50AU}{R} \right)^{1/2} \left(\frac{M}{0.5M_{\odot}} \right)^{1/2}, \quad (12)$$

we see that for values typical of what is observationally inferred for the stellar mass and position and temperature of accretion disk walls in T Tauri protoplanetary disks, those indicated in the above equation (e.g., D'Alessio et al. 2005; Espaillat et al. 2007; Hughes et al. 2009), one approaches the breakdown of the thin disk approximation, $\mathcal{M} < 1$, and consequently the transition to radial flow.

Taking typical inferred values for R/H at the wall of ~ 5 (e.g., D'Alessio et al. 2005; Espaillat et al. 2007; Hughes et al. 2009), we can now write the condition for the transition to radial flow, locally at the wall, as:

$$10 = 6\pi\alpha(n - 1/2). \quad (13)$$

We see that for a standard value of $n \sim 1$ the above equation implies a reasonable value of $\alpha \sim 1$ at the thick wall, significantly higher than the values of ~ 0.01 and lower, which apply for the body of the thin accretion disk beyond this radius. A substantial increase of α as R/H decreases is expected in any turbulence driven viscosity model for accretion disks, e.g., Firmani, Hernández, & Gallagher (1996), in the context of galactic disks.

In terms of the debate surrounding the inference of inner holes in observed accretion disks, many solutions have been proposed in terms of disk clearing mechanisms; grain growth (e.g., Strom et al. 1989; Dullemond & Dominik 2005), photoevaporation (e.g., Clarke, Gendrin, & Sotomayor 2001), magnetorotational instability inside-out clearing (e.g., Chiang & Murray-Clay 2007; Dutrey et al. 2008), binarity (e.g., Ireland & Kraus 2008) and planet-disk interactions (e.g., Rice et al. 2003). None of the above is entirely satisfactory, as noted by Hughes et al. (2009), mostly due to their incompatibility with a steady state solution. An alternative solution under the proposed scenario, is that there is no actual disk material clearing, only a transition to predominantly radial flow at the thick wall, and consequently a shear-free flow interior to this point. Once the disk heating mechanism is removed, as one should expect from the analysis presented in this section, the inner disk disappears from sight.

This transition at a thickened inner boundary is qualitatively what ADAF models propose. In those models, substantial turbulent and thermal pressure remain within the inner flow. Still, given the present lack of a definitive jet generation mechanism, we consider it interesting to explore the consequences of a model where cooling drives the flow to a $\nabla P_0/\rho \ll \nabla \Phi$ condition. As we show in the following sections, we prove that such a situation will quite naturally yield purely hydrodynamical jet solutions, which we find encouraging.

3. HYDRODYNAMICAL JET SOLUTIONS

We shall now model the physical situation resulting from the scenario described above as an axially symmetrical distribution of gas in free fall towards a central star of mass M . Taking a spherical coordinate system with θ the angle between the positive vertical direction and the position vector \vec{r} we have:

$$\frac{1}{r^2} \frac{\partial(r^2 \rho V)}{\partial r} + \frac{1}{r \sin(\theta)} \frac{\partial(\sin(\theta) \rho U)}{\partial \theta} = 0, \quad (14)$$

$$V \frac{\partial V}{\partial r} + \frac{U}{r} \frac{\partial V}{\partial \theta} - \frac{U^2}{r} = -\frac{1}{\rho} \frac{\partial P}{\partial r} - \frac{GM}{r^2}, \quad (15)$$

$$V \frac{\partial U}{\partial r} + \frac{U}{r} \frac{\partial U}{\partial \theta} + \frac{VU}{r} = -\frac{1}{r\rho} \frac{\partial P}{\partial \theta}, \quad (16)$$

for the continuity equation, and the radial and angular components of Euler's equation. In the above, V , U , ρ and P give the radial velocity, angular velocity, matter density and pressure, respectively. We have neglected temporal derivatives, as we are interested at this point, in the characteristics of steady state solutions, although the temporal derivatives are reinstated in the Appendix for the purpose of stability analysis. We take as a background state a free-falling axially symmetrical distribution of gas described by $V_0 = -(2GM/r)^{1/2}$, $U_0 = 0$ and all components of $\nabla P_0/\rho_0$ negligible, a consistent solution to equations(15) and (16), used only in the

description of this background. Having ignored the inclusion of the radius at which the transition to radial flow takes place in the choice of V_0 limits the validity of the analysis to radial scales along the plane of the disk much smaller than R_T . This is justified by the fact that jets appear as phenomena extremely localised towards $R \rightarrow 0$. We now take a density profile given by:

$$\rho_0(r, \theta) = f(r)g(\theta), \quad (17)$$

where $f(r)$ is a dimensionless function of r and $g(\theta)$ describes the polar angle dependence of the infalling material, for example, one can ask for $g(\theta = \pi/2) = \bar{\rho}_0$, diminishing symmetrically towards the poles. The choice of this last function will determine the details of the problem, and can be thought of as something of the type

$$g(\theta) = \bar{\rho}_0 e^{-\left(\frac{\theta - \pi/2}{\sqrt{2}\theta_0}\right)^2} \quad (18)$$

with $\bar{\rho}_0$ a normalisation constant and θ_0 a form constant describing the flattening of the disk of infalling material. However, we shall mostly leave results indicated in terms of $g(\theta)$. The continuity equation (14) now fixes $f(r)$ through:

$$-\frac{g(\theta)}{r^2} \frac{d}{dr} \left[(2GM)^{1/2} r^{3/2} f(r) \right] = 0, \quad (19)$$

and hence $f(r)r^{3/2} = \text{constant}$, which completes the description of the background state through:

$$\rho_0(r, \theta) = \left(\frac{\bar{r}}{r}\right)^{3/2} g(\theta), \quad (20)$$

with \bar{r} a constant which determines the point at which $g(\theta = \pi/2) \Rightarrow \rho_0 = \bar{\rho}_0$.

We now study the first order departures from the assumed background state through a perturbative approach, to explore the possibility that such departures might naturally give rise to a hydrodynamical jet. Regarding these first order perturbations, we shall also be interested in steady state solutions given by:

$$V(r, \theta) = V_0(r) + V_1(r, \theta), \quad (21)$$

$$U(r, \theta) = 0 + U_1(r, \theta), \quad (22)$$

$$\rho(r, \theta) = \rho_0(r, \theta) + \rho_1(r, \theta), \quad (23)$$

where quantities with subscript (1) denote the perturbation on the background solution. Notice that V_0 is, as required by the assumed background state, a function only of the radial coordinate r . For the background state assumed, the perturbations on it will be solved for in a fully self-consistent manner. Writing equations (14), (15) and (16) to first order in the perturbation one obtains after rearranging terms:

$$g(\theta) \frac{\partial (r^{1/2} V_1)}{\partial r} - B \frac{\partial (r^{3/2} \rho_1)}{\partial r} = \frac{-1}{r^{1/2} \sin(\theta)} \frac{\partial (\sin(\theta) g(\theta) U_1)}{\partial \theta}, \quad (24)$$

$$\frac{\partial (V_1/r^{1/2})}{\partial r} = \frac{Ar^{3/2}}{g(\theta)} \frac{\partial \rho_1}{\partial r}, \quad (25)$$

$$\frac{\partial (rU_1)}{\partial r} = \frac{Ar^2}{g(\theta)} \frac{\partial \rho_1}{\partial \theta}, \quad (26)$$

In the above we have assumed an isothermal equation of state for the perturbation $P_1 = c^2 \rho_1$, an assumption often used in the modeling of astrophysical jets, e.g., the T Tauri jets observed and modelled by Hartigan, Edwards, & Pierson (2004). This idealised case serves to illustrate clearly the consequences of the physical setup being considered, as it allows for an analytic solution. The generalisation to more realistic adiabatic, polytropic or other equations of state can be performed numerically, and can be expected to yield qualitatively similar results, although interesting differences in the details can be expected to emerge, which will be considered later. In the above three equations we have introduced the constants $A = (c^4/2GM\bar{r}^3)^{1/2}$ and $B = (2GM/\bar{r}^3)^{1/2}$.

To make further progress we can attempt a solution through the method of separation of variables, proposing a solution of the form: $V_1 = V_r V_\theta$, $U_1 = U_r U_\theta$, $\rho_1 = \rho_r \rho_\theta$. This ansatz yields two independent systems of

three equations each, one for the radial, and one for the angular dependences of the perturbations. The radial equations become:

$$\frac{d(V_r/r^{1/2})}{dr} = C_r r^{3/2} \frac{d\rho_r}{dr}, \quad (27)$$

$$\frac{d(rU_r)}{dr} = C_\theta r^2 \rho_r, \quad (28)$$

$$\frac{d(r^{1/2}V_r)}{dr} - \left(\frac{BC_r}{A}\right) \frac{d(r^{3/2}\rho_r)}{dr} = C_c \frac{U_r}{r^{1/2}}, \quad (29)$$

where we have used the results of the angular ones:

$$V_\theta g(\theta) = \left(\frac{A}{C_r}\right) \rho_\theta, \quad (30)$$

$$\frac{d\rho_\theta}{d\theta} = \left(\frac{C_\theta}{A}\right) g(\theta) U_\theta, \quad (31)$$

$$\frac{d(\sin(\theta)g(\theta)U_\theta)}{d\theta} = -C_c \sin(\theta)g(\theta)V_\theta. \quad (32)$$

In splitting the radial and angular dependences of the perturbed continuity equation, equation (24), we have used the result of the angular equation of the perturbed radial Euler equation, equation (30). The constants C_r , C_θ and C_c are the separation constants of the problem. Firstly we turn to the angular system, which allows an exact solution.

We can take equation (32) and substitute into it the product $g(\theta)U_\theta$ from equation (31), and the product $g(\theta)V_\theta$ from equation (30) to obtain an equation involving only ρ_θ :

$$\frac{d^2\rho_\theta}{d\theta^2} + \cot(\theta) \frac{d\rho_\theta}{d\theta} + \left(\frac{C_c C_\theta}{C_r}\right) \rho_\theta = 0, \quad (33)$$

having solution:

$$\rho_\theta = c_1 P_m(\cos(\theta)) + c_2 Q_m(\cos(\theta)). \quad (34)$$

In the above equation c_1 and c_2 are normalisation constants, and P_m and Q_m are the Legendre polynomials of the first and second kinds, respectively. The index of these functions is given by the relation $2m = (4C_T + 1)^{1/2} - 1$, where $C_T = (C_c C_\theta / C_r)$. As typical of separation of variables problems, we see the solution as an eigenvalue problem, with the separation constants determining the order of the solution function. The requirement of axial symmetry forces m to be even. Any such desired angular distribution for ρ_θ can now be constructed as an infinite series of the above functions. For simplicity we analyse the case of $m = 2$ ($C_T = 6$), $c_1 = \bar{\rho}_\theta$, $c_2 = 0$:

$$\rho_\theta = \bar{\rho}_\theta (3\cos^2(\theta) - 1). \quad (35)$$

This will result in slightly less material along the plane of the disk, and slightly more along the poles, for the total density $\rho = \rho_0 + \rho_1$, with respect to the background state ρ_0 . At this point equations (30) and (31) can be used to obtain:

$$V_\theta = \left(\frac{A\bar{\rho}_\theta}{C_r}\right) \left(\frac{3\cos^2(\theta) - 1}{g(\theta)}\right), \quad (36)$$

$$U_\theta = -\left(\frac{6A\bar{\rho}_\theta}{C_\theta}\right) \left(\frac{\cos(\theta)\sin(\theta)}{g(\theta)}\right). \quad (37)$$

We see the potential for jet formation already in the two above equations; if the background state is relatively devoid of material towards the poles, $g(\theta)$ could be small for $\theta = 0$, $\theta = \pi$ and equation (36) will lead to large radial velocities along the poles. Further, equation (37) shows that the angular velocity will always tend to zero both on the plane of the disk, and along the poles, where movement will necessarily be radial, although not necessarily positive.

The case of the radial system is more cumbersome, as the linear operator which appears is of third order. However, in the Appendix we show through a first order stability analysis which terms can be safely ignored in the high-frequency approximation, and for small r , the region where jets develop. Equation (58) is used to show that the right-hand side of equation (29) can be ignored to leading order, so that the resulting equation can be readily integrated to give:

$$V_r = \left(\frac{BC_r}{A} \right) r \rho_r. \quad (38)$$

In the above we have taken the integration constant which appears as being equal to zero, from requiring $V_r \rightarrow 0$ for $\rho_r \rightarrow 0$. Substituting the above relation for V_r into equation (27) leads to:

$$\frac{d\rho_r}{dr} \left[\left(\frac{B}{A} \right) r - r^2 \right] + \left(\frac{B}{A} \right) \frac{\rho_r}{2} = 0. \quad (39)$$

We see from equation (59) in the Appendix that the second term on the left-hand side of the above equation can be dismissed, to leading order, in the regime of validity there established. We then obtain:

$$\rho_r = \bar{\rho}_r \left(\frac{\bar{r}_\rho}{r} \right)^{1/2}, \quad (40)$$

$$V_r = \left(\frac{BC_r}{A} \right) \bar{\rho}_r \bar{r}_\rho^{-1/2} r^{1/2}, \quad (41)$$

where \bar{r}_ρ is a characteristic radius at which $\rho_r = \bar{\rho}_r$. Now from equation (28), where all the terms are of the same order, as is shown in equation (62), we have

$$U_r = \left(\frac{2C_\theta \bar{\rho}_r \bar{r}_\rho^{-1/2}}{5} \right) r^{3/2}. \quad (42)$$

In the above equation we have also taken the integration constant as zero, from requiring $U_r \rightarrow 0$ for $r \rightarrow 0$. Choosing without loss of generality the two characteristic radii \bar{r} and \bar{r}_ρ both equal to GM/c^2 , we can now write the full solution to the perturbation as:

$$\rho_1 = \bar{\rho}_J \left(\frac{GM}{c^2 r} \right)^{1/2} (3\cos^2(\theta) - 1), \quad (43)$$

$$V_1 = c \left(\frac{\bar{\rho}_J}{\bar{\rho}_0} \right) \left(\frac{2c^2 r}{GM} \right)^{1/2} \left(\frac{3\cos^2(\theta) - 1}{g_\theta} \right), \quad (44)$$

$$U_1 = -c \left(\frac{3\bar{\rho}_J}{5\bar{\rho}_0} \right) \left(\frac{2c^2 r}{GM} \right)^{3/2} \left(\frac{\cos(\theta)\sin(\theta)}{g_\theta} \right), \quad (45)$$

where we have introduced $\bar{\rho}_J = \bar{\rho}_\theta \bar{\rho}_r$ and g_θ as the angular part of $g(\theta)$, $g(\theta)/\bar{\rho}_0$. The full solution to the perturbation can be seen to depend only on the two parameters $\bar{\rho}_0$ and $\bar{\rho}_J$, normalisation constants for the densities of the background state and the perturbation, with the velocities of the perturbation solution depending only, and linearly, on the ratio $Q = 2^{1/2} \bar{\rho}_J / \bar{\rho}_0$, which determines the validity regime of the perturbative approach through the condition $Q < 2^{1/2}$.

As was already evident from equation (37), we see from equation (45) that the angular velocity will be zero only for $\theta = \pi/2$, $\theta = 0$ and $\theta = \pi$. Thus, movement along the plane of the disk will remain along the plane, but also, along the poles movement will be exclusively radial. This last point, together with the positive sign of the radial velocity along the poles (c.f. equation (44) for $\theta = 0$), provides for a well collimated jet along the poles. Hence, the background state proposed is seen to be unstable towards jet formation.

From equation (44) we see that one has only to ask for a background state where matter density does not grow towards the poles in order to obtain ejection velocities along them, which could become very large for flattened disks with relatively empty poles. The axial symmetry condition imposed on equation (34) guarantees both axial symmetry and symmetry above and below the plane of the disk for the full solution. We see also that

if one takes higher orders for m , the index of the Legendre polynomial solution to equation (33), one obtains increasingly more critical angles at positions intermediate between 0 and $\pi/2$ at which the angular velocity goes to zero. In fact, more complex geometries and asymmetric jets appear, as inferred observationally by e.g., Ferreira et al. (2006), if m is taken as an arbitrary real number. However, modelling a situation where a polar jet dominates the ejection identifies $m = 2$ as the leading order.

Notice that the qualitative behaviour of the solution is guaranteed by the exactness of the angular solution; the approximation $r < 2GM/c^2$ used for solving the radial problem will only introduce an error in the magnitudes of the velocities outside of $r < 2GM/c^2$, but will not change the fact that velocities will be of radial infall along the plane of the disk, $\theta = \pi/2$, and of radial outflow along the poles, the jet solution for $\theta = 0, \pi$. This is reinforced by the stability analysis performed in the Appendix, where we show that the angular system of equations does not respond to a temporal perturbation to the first order solution treated here, while the response of the radial system is merely the introduction of periodic and bound factors multiplying the radial solutions given in this section.

The two constants of the problem, $\bar{\rho}_0$ and $\bar{\rho}_J$, can be calculated once a choice of $g(\theta)$ is specified, from the two conditions:

$$\dot{M}_a = 2\pi \int_0^\pi \rho_0 V_0 \sin(\theta) r^2 d\theta, \quad (46)$$

$$\dot{M}_j = 2\pi \int_0^{\theta_J} \rho_1 V_1 \sin(\theta) r^2 d\theta, \quad (47)$$

where θ_J is a suitable angle defining the opening of the jet, in all likelihood very small, as will be seen in the following section. In the above equations \dot{M}_a gives the matter accretion rate onto the central star, and \dot{M}_j the matter ejection rate due to the jet. Dimensionally, the two quantities above will scale as:

$$\dot{M}_a = C_a \frac{(\pi GM)^2}{c^3} \bar{\rho}_0, \quad (48)$$

$$\dot{M}_j = C_j \frac{(\pi GM)^2}{c^3} \frac{\bar{\rho}_J^2}{\bar{\rho}_0}, \quad (49)$$

where C_a and C_j are two dimensionless constants which will depend on the choice of g_θ , and which would be expected to be of order 1.

Qualitatively, this type of model naturally furnishes a tight disk-jet connection (c.f. equation 44) e.g., as now firmly established in microquasars and AGN jets (see e.g., Marscher et al. 2002; Chatterjee et al. 2009). In the above systems bursts of enhanced jet activity are seen to follow temporal dips in disk luminosity output after small characteristic delay times. In the present model, such a situation would be expected if the critical radius for transition to radial flow in the disk made a sudden transition to higher values. Again, the drop in disk output might not reflect the disk material disappearing (in this case being swallowed by the central black hole, as sometimes proposed), but simply fading from view as heating mechanisms shut down, then naturally enhancing jet activity as the effective \dot{M}_a increases.

4. PARTICULAR SOLUTIONS

In order to present a sample of the trajectories expected in the model, we turn to the full solution to the problem for $m = 2$, equations (21) and (22), but written in dimensionless form:

$$\frac{d\mathcal{R}}{d\mathcal{T}} = \frac{-1}{\mathcal{R}^{1/2}} + Q\mathcal{R}^{1/2} \left(\frac{3\cos^2(\theta) - 1}{g_\theta} \right), \quad (50)$$

$$\frac{d\theta}{d\mathcal{T}} = -\frac{6}{5}Q\mathcal{R}^{1/2} \left(\frac{\sin(\theta)\cos(\theta)}{g_\theta} \right). \quad (51)$$

The above remain in spherical coordinates, where $\mathcal{R} = rc^2/GM$ and $\mathcal{T} = tc^3/GM$. Notice that the threshold for jet development can now be stated as the condition $d\mathcal{R}/d\mathcal{T} > 0$, $Q\mathcal{R}(3\cos^2(\theta) - 1) > g_\theta$. A choice of Q and g_θ now allows to numerically integrate trajectories. We take:

$$g_\theta = e^{-\left(\frac{\theta - \pi/2}{\sqrt{2}\theta_0}\right)^2}, \quad (52)$$

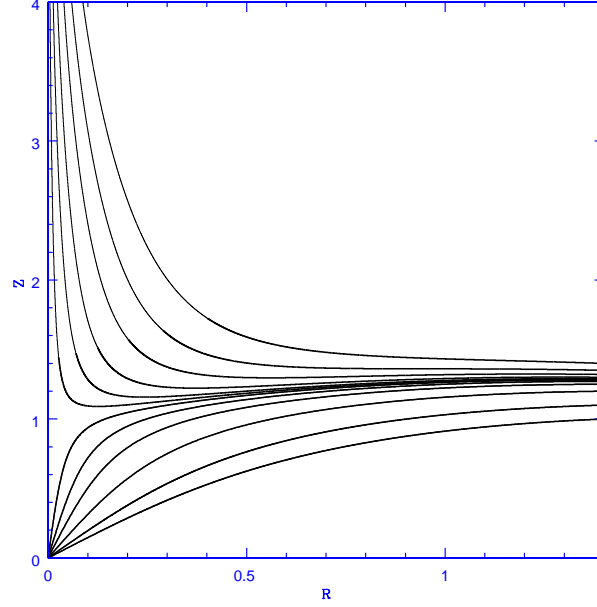


Fig. 1. Trajectories for the complete solution, for a range of initial vertical height positions at $\mathcal{R} = 1.4$. The dimensionless parameters of the problem were chosen as $\theta_0 = \pi/2$, $Q = 0.3$. We see the lowermost six trajectories converging onto the central potential, but the six upper ones shooting up into a polar jet, with velocities exceeding the local escape velocities.

as a model for the background state, where small values of θ_0 will result in thin disks, while more spherical mass distributions correspond to large values of θ_0 . As a first example we take $Q = 0.3$ ($\bar{\rho}_J/\bar{\rho}_0 = 0.2$) and $\theta_0 = \pi/2$, a fairly thick disk, with only very small changes in density from the plane to the poles of a factor of 1.6, an almost spherically symmetric density configuration compatible with what appears in some ADAF models. This value of θ_0 is far from representing a flattened disk, and hence one which does not force the jet solution, see equation (44). With these parameters, and initial conditions specified in dimensionless cylindrical coordinates as $\mathcal{R} = 1.4$ and Z ranging from 1.0 to 1.4, we solve equations (50) and (51) through a finite differences scheme to plot Figure 1.

In spite of having taken $\bar{\rho}_J/\bar{\rho}_0 < 1$, the validity of the perturbative approach could be broken by the appearance of large velocities in the perturbation, breaking the validity condition $V_1/V_0 < 1$. We explicitly keep track of this condition, and show the appearance of perturbation radial velocities violating it with a change to thin lines in Figure 1; angular velocities for the perturbation will always remain of order Q , provided $\mathcal{R} < 1$.

For this case, the two lowermost curves present trajectories which all turn downwards to converge onto the central star. These are solutions which essentially follow the background state, infalling onto the bottom of the potential well. As one raises the initial value of Z however, the following 4 curves begin to increasingly deviate from the free fall trajectories and, although still ending up at $\mathcal{R} = 0$, clearly show a change in behaviour. A threshold is eventually crossed and curves of a very different type ensue, the six upper jet trajectories shown in Figure 1. We see the pressure gradients associated with the distribution of matter in the background solution acting to break the fall of the incoming material, turn it back, and then accelerate it vertically through the vertical density gradients. These jet trajectories rapidly converge with height to eventually yield a well collimated structure.

Note that the region where the perturbation condition $V_1 < V_0$ ceases to be valid appears only on the “jet” trajectories, and only after these have turned upwards, at points where in fact, velocities already exceed the local escape velocities. This point guarantees the appearance of a jet, even though the details of the flow in this jet region could differ somewhat from what is shown by the thin lines in the figure. The same applies to the $\mathcal{R} < 2$ validity region of the radial equation: the jet solution appears within the validity regime of all the approximations taken. the qualitative form of the full solution will not deviate much from what is shown in Figure 1, due to the exact character of the angular solution.

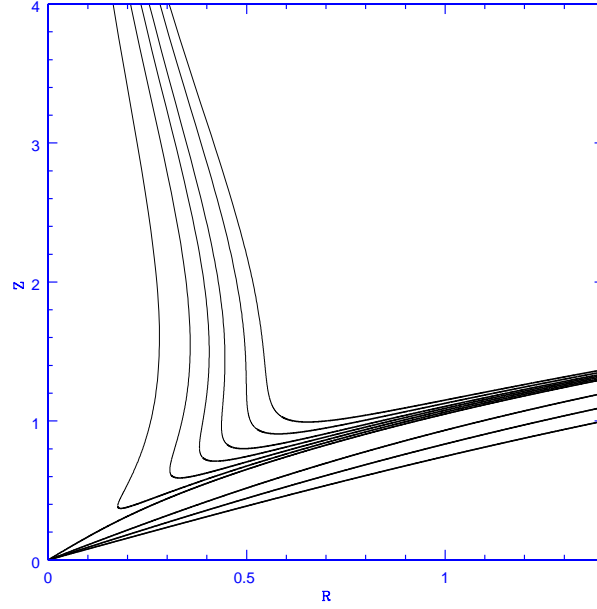


Fig. 2. Trajectories for the complete solution, for a range of initial vertical height positions at $\mathcal{R} = 1.4$. The dimensionless parameters of the problem were chosen as $\theta_0 = \pi/9$, $Q = 0.01$. We see the lowermost four trajectories converging onto the central potential, but the six upper ones shooting up into a polar jet, with velocities exceeding the local escape velocities.

Notice that the generic validity of the solution proposed does not require that all of the disk material should lose all of its angular momentum at the critical radius R_T , only that some of the disk material should lose most of its angular momentum at that point. Any minor, residual angular momentum remaining on the disk fraction which forms the jet will only establish a finite jet cross-sectional area through the appearance of a centrifugal barrier, which will present only a small correction on the scenario given here. Still, the empirical presence of spectroscopically studied accretion disks truncated interior to certain critical radii suggests the very substantial reduction of the shears in that region, as could happen if a transition to mostly radial flow takes place.

Going back to equations (50) and (51) we see that one expects

$$Q^2 \sim \frac{\dot{M}_j}{\dot{M}_a}. \quad (53)$$

It is reassuring that for the jets associated with T Tauri stars for example, values of \dot{M}_j/\dot{M}_a of between 0.1 and 0.01 on average are observationally inferred and therefore of order $0.3 < Q < 0.1$ (e.g., Hartigan, Edwards, & Gandhour 1995; Gullbring et al. 1998; Hartigan et al. 2004; Ferreira et al. 2006). These are compatible with the value used to plot Figure 1, and hence ones which will readily yield jet solutions.

Figure 2 is analogous to Figure 1, but presents an example for a much more flattened disk having $\theta_0 = \pi/9$, a significantly flattened disk where the density contrast between plane and pole at fixed radius is now of a factor of 2.5×10^4 , orders of magnitude larger than in the last example. We take this time $Q = 10^{-2}$. Again, we see the main features of the solution being well established in the region interior to $\mathcal{R} < 2$, with a jet solution again established within the validity regime of all approximations used.

The long range stability and coherence of these structures lies outside the scope of this work, and is in all probability furnished by a series of mechanisms extensively explored in the literature including angular momentum, magnetic fields and pressure containment of the surrounding medium, e.g., Begelman, Blandford, & Rees (1984), Blandford (1990), Falle (1991), Kaiser & Alexander (1997).

In going to the more extreme jet phenomena associated with stellar black holes (e.g., Mirabel & Rodríguez 1999), quasars (e.g., Marscher et al. 2002) and gamma ray bursts (e.g., Mészáros 2002), it is natural to expect the ideas presented here to apply, but amplified to a much more extreme regime by the appearance of corresponding relativistic and general relativistic effects, to first order, the shift in the divergence in the

potential from $r = 0$ in the Newtonian case to $r = r_s$ in the general relativistic one. It is therefore natural to expect a purely hydrodynamic jet generation mechanism to apply across all classes of astrophysical objects, specially given the qualitative scalings and similarities which appear over all astrophysical jet classes (e.g., Mirabel & Rodríguez 1999; Mendoza, Hernández, & Lee 2005), in addition to the magnetically driven processes traditionally found in the literature.

Notice from equation (44) the intimate link between the jet velocity and the physical state of the infalling material, c and \dot{M}_a through $\bar{\rho}_0$. This implies that temporal variations in the parameters of the infalling material will result in temporal variations in the density and velocity of the jet material, in a way described by equations(43) and (44). The above can serve as a physical description of the key processes relevant to the formation of internal shocks in astrophysical jets, the main ingredient behind phenomena such as HH objects and gamma ray bursts.

Although the solution to the problem presented is rigorous, and the appearance of the resulting hydrodynamical jets solid, the relevance of our model is clearly constrained by the validity, or otherwise, of the starting hypothesis; most critically, the appearance of an inner region in free fall. Although plausibility arguments for the appearance of this regime have been given, the reality of it is certainly not assured. Still, given the absence of a fully satisfactory and general solution to the problem of jet generation, and given the clear and transparent physics of the one shown here, we believe it is interesting to present such a simple hydrodynamical jet solution.

5. CONCLUSIONS

We show that given a radially infalling accretion, a purely hydrodynamical jet ensues.

We calculate the condition for the transition from quasi-circular to quasi-radial flow in a standard accretion disk, and show it will always occur for power law surface density profiles of the form $\Sigma \propto R^{-n}$, interior to a critical radius, provided $n > 1/2$.

Comparison with inferred inner holes in observed accretion disks yields results consistent with our estimates for the above transition radius, the point where shears in the flow would be substantially reduced.

Well collimated jets readily appear, proving the existence of purely hydrodynamical mechanisms for the generation of astrophysical jets.

Xavier Hernández acknowledges the hospitality of the Observatoire de Paris for the duration of a sabbatical stay during which many of the ideas presented here were first developed, and financial support from project PAPIIT IN103011 DGAPA Universidad Nacional Autónoma de México. Pablo L. Rendón and Rosa Rodríguez acknowledge financial support from project PAPIIT IN110411 DGAPA Universidad Nacional Autónoma de México. Antonio Capella acknowledges financial support from project PAPIIT IN101410 DGAPA Universidad Nacional Autónoma de México.

APPENDIX: STABILITY ANALYSIS

We study the stability of the system by means of a standard linear perturbation approach. Furthermore, we develop here a first order analysis that also serves to justify the approximations made in § 3 of the main body of the paper. We follow the approach used by Papaloizou & Pringle (1984) to study the stability of this system by means of linear perturbation of the time-dependent equations of the fluid, as opposed to the steady-state versions stated previously as equations (24)–(26). The time-dependence of the perturbed quantities is written as $\exp(i\omega t)$, where ω is a temporal frequency. We then obtain

$$i\omega\rho_1 \frac{r^2}{\bar{r}^{3/2}} + g(\theta) \frac{\partial (r^{1/2}V_1)}{\partial r} - B \frac{\partial (r^{3/2}\rho_1)}{\partial r} = \frac{-1}{r^{1/2}\sin(\theta)} \frac{\partial (\sin(\theta)g(\theta)U_1)}{\partial \theta}, \quad (54)$$

for the continuity equation, and

$$i\omega \left(\frac{1}{2GM} \right)^{1/2} V_1 + \frac{\partial (V_1/r^{1/2})}{\partial r} = \frac{Ar^{3/2}}{g(\theta)} \frac{\partial \rho_1}{\partial r}, \quad (55)$$

$$-i\omega r \left(\frac{1}{2GM} \right)^{1/2} U_1 + \frac{\partial (rU_1)}{\partial r} = \frac{Ar^2}{g(\theta)} \frac{\partial \rho_1}{\partial \theta}, \quad (56)$$

for the radial and angular components of the Euler equation, respectively. We now proceed as before, separating variables in such a way that we require the angular components ρ_θ , V_θ and U_θ to be dimensionless, while the radial components ρ_r , V_r and U_r have the same dimensions as the original functions. Encouragingly, the equations for the angular components are exactly the same as those obtained for the steady-state analysis, equations (30)–(32). We conclude that the angular components are not time-dependent and are thus unconditionally stable, reinforcing the overall character of the solution presented in § 3. The resulting equations for the radial components do include an extra term due to the temporal dependence. In order to establish the relative magnitude of the different terms in these equations, we shall rewrite them in dimensionless form, using the following scalings for that effect:

$$r^* = \frac{r}{r_0}, \quad \rho^* = \frac{\rho_r}{\rho_0}, \quad V^* = \frac{V_r}{\omega \bar{r}}, \quad U^* = \frac{U_r}{\omega r_0}, \quad (57)$$

where ρ_0 is a characteristic density, $\bar{r} = 2GM/c^2$, and $r_0 = (2GM/\omega^2)^{1/3}$. We now consider the high-frequency limit, as Papaloizou & Pringle (1984) have also done. Notice then that $\epsilon = r_0/\bar{r} = c^2/(2GM\omega)^{2/3} \ll 1$. equation (54) may now be rewritten as

$$\frac{\partial(r^{*1/2}V^*)}{\partial r^*} - \beta \frac{\partial(r^{*3/2}\rho^*)}{\partial r^*} + i\beta r^{*2}\rho^* = \epsilon C_c \frac{U^*}{r^{*1/2}}, \quad (58)$$

where $\beta = C_r \rho_0 (2GM/\omega^5)^{1/3}$. If we now require $C_c \sim 1$ and $C_r \sim \rho_0^{-1}(\omega^5/2GM)^{1/3}$, we observe that all the terms on the left-hand side of the equation are $O(1)$, whereas the term on the right-hand side is $O(\epsilon)$. Thus, at leading order the term on the right-hand side vanishes.

Using this same scaling, equation (55) is now

$$\frac{\partial(r^{*-1/2}V^*)}{\partial r^*} + iV^* = \epsilon \beta r^{*3/2} \frac{\partial \rho^*}{\partial r^*}, \quad (59)$$

where we observe that the term on the right-hand side is $O(\epsilon)$. Again, at $O(1)$, the right-hand side of the equation vanishes, and we may solve the equation to obtain

$$V^* = \alpha_1 r^{*1/2} \exp\left(-i\frac{2}{3}r^{*3/2}\right), \quad (60)$$

where α_1 is a constant. Substituting the real part of solution (60) in (58) we now solve for ρ^* ,

$$\rho^* = \frac{\alpha_1}{2\beta r^{*1/2}} \left[\exp\left(i\frac{2}{3}r^{*3/2}\right) + \frac{1}{2} \exp\left(-i\frac{2}{3}r^{*3/2}\right) \right] + \alpha_2 r^{*-3/2} \exp\left(-i\frac{2}{3}r^{*3/2}\right) + \frac{i\alpha_1 r^*}{5\beta} \exp\left(i\frac{2}{3}r^{*3/2}\right) + \frac{i^{4/3}\alpha_1}{4 \cdot 6^{1/3} \beta r^{*3/2}} \exp\left(i\frac{2}{3}r^{*3/2}\right) \Gamma\left(\frac{2}{3}, i\frac{4}{3}r^{*3/2}\right), \quad (61)$$

where α_2 is a constant, and Γ is the incomplete gamma function. The real parts of these solutions are the dimensionless forms of the solutions we obtained for V_r and ρ_r in § 3 of this paper, modulated by an oscillating and bounded function.

Finally, in dimensionless form, equation (56) is

$$\frac{\partial(r^*U^*)}{\partial r^*} - i r^{*3/2} U^* = \beta' r^{*2} \rho^*. \quad (62)$$

where $\beta' = C_\theta \rho_0 (2GM/\omega^5)^{1/3}$. If we now require $C_\theta \sim \rho_0^{-1}(\omega^5/2GM)^{1/3}$, all three terms are $O(1)$. Notice that the orders of magnitude chosen here for the separation constants give as a result $C_T \sim 1$, so that the choice of value given to C_T in § 3 is consistent with our analysis. Taking the real part of the solution given in (61) and substituting in the above equation, we may solve to obtain

$$U^* = \exp\left(i\frac{2}{3}r^{*3/2}\right) \left[\frac{\alpha_3}{r^*} + \frac{1}{10} \frac{\alpha_1 \beta'}{\beta} r^{*3/2} \right] + \frac{\alpha_1 \beta'}{\beta} \frac{i^{1/3}}{8 \cdot 6^{1/3} r^*} \exp\left(i\frac{2}{3}r^{*3/2}\right) \Gamma\left(\frac{2}{3}, i\frac{4}{3}r^{*3/2}\right) + \frac{\alpha_1 \beta' i}{\beta} \frac{1}{8} \exp\left(-i\frac{2}{3}r^{*3/2}\right), \quad (63)$$

where α_3 is a constant. Considering the real part of the above solution, we again find that we have the dimensionless form of the solution obtained for U_r earlier in this paper, modulated by an oscillating, bounded function.

Thus, the effect of linear perturbations on the time-dependent system is to provoke bounded oscillations around the steady-state solutions for density and both angular and radial velocities. We conclude that the system is neutrally stable.

Our choice of scalings has permitted us to write the equations of the fluid in dimensionless form in terms of only three dimensionless parameters, ϵ , β and β' . In this form, as is expected, it becomes rather more straightforward to establish the leading-order terms in the equations. The hypothesis of small radial distance translates into the smallness of ϵ , and β and β' , formally very similar, are related to the separation constants. It should be pointed out that the dimensional constants C_r and C_θ are independently required to be of the same order, and by simply letting the dimensionless constant C_c be $O(1)$, the sole restriction placed upon these three constants in § 3, that C_T also be $O(1)$, is fulfilled. We can then consistently fix the order of the Legendre polynomial solutions presented in § 3 as a function of the particular values given to the separation constants, a behaviour typically associated with the method of separation of variables.

REFERENCES

- Begelman, M., Blandford, R. D., & Rees, M. 1984, *Rev. Mod. Phys.*, 56, 255
- Blandford, R. D. 1990, in *Active Galactic Nuclei*, ed. Courvoisier, T. L., Mayor, M. (Berlin: Springer-Verlag), 161
- Blandford, R. D., & Payne, D. G. 1982, *MNRAS*, 199, 883
- Chatterjee, R., et al. 2009, *ApJ*, 704, 1689
- Chiang, E., & Murray-Clay, R. 2007, *Nature Phys.*, 3, 604
- Clarke, C. J., Gendrin, A., & Sotomayor, M. 2001, *MNRAS*, 328, 485
- D'Alessio, P., et al. 2005, *ApJ*, 621, 461
- Dullemond, C. P., & Dominik, C. 2005, *A&A*, 434, 971
- Dutrey, A., et al. 2008, *A&A*, 490, L15
- Espaillat, C., et al. 2007, *ApJ*, 670, L135
- Falle, S. A. E. G. 1991, *MNRAS*, 250, 581
- Ferreira, J., Dougados, C., & Cabrit, S. 2006, *A&A*, 453, 785
- Firmani, C., Hernández, X., & Gallagher, J. 1996, *A&A*, 308, 403
- Glauert, M. B. 1956, *J. Fluid Mech.*, 1, 625
- Gullbring, E., Hartmann, L., Briceño, C., & Calvet, N. 1998, *ApJ*, 492, 323
- Hartmann, L., Calvet, N., Gullbring, E., & D'Alessio, P. 1998, *ApJ*, 495, 385
- Hartigan, P., Edwards, S., & Gandhour, L. 1995, *ApJ*, 452, 736
- Hartigan, P., Edwards, S., & Pierson, R. 2004, *ApJ*, 609, 261
- Henriksen, R. N., & Valls-Gabaud, D. 1994, *MNRAS*, 266, 681
- Hughes, A. M., et al. 2009, *ApJ*, 698, 131
- Ireland, M. J., & Kraus, A. L. 2008, *ApJ*, 678, L59
- Kaiser, C. R., & Alexander, P. 1997, *MNRAS*, 286, 215
- King, A. C., & Needham, D. J. 1994, *J. Fluid Mech.*, 268, 89
- Lada, C., et al. 2006, *AJ*, 131, 1574
- Marscher, A. P., Jorstad, S. G., Gomez, J., Aller, M. F., Teräsrananta, H., Lister, M. L., & Stirling, A. M. 2002, *Nature*, 417, 625
- Meier, D. L., Koide, S., & Uchida, Y. 2001, *Science*, 291, 84
- Mendoza, S., Hernández, X., & Lee, W. H. 2005, *RevMA*, 41, 453
- Mészáros, P. 2002, *ARA&A*, 40, 137
- Mirabel, I. F., & Rodríguez, L. F. 1999, *ARA&A*, 37, 409
- Papaloizou, J. C. B., & Pringle, J. E. 1984, *MNRAS*, 208, 721
- Price, D. J., Pringle, J. E., & King, A. R. 2003, *MNRAS*, 339, 1223
- Pringle, J. E. 1981, *ARA&A*, 19, 137
- Reipurth, B., & Bally, J. 2001, *ARA&A*, 39, 403
- Rice, W. K. M., Wood, K., Armitage, P. J., Whitney, B. A., & Bjorkman, J. E. 2003, *MNRAS*, 324, 79
- Shakura, N. I., & Sunyaev, R. A. 1973, *A&A*, 24, 337
- Scheuer, P. A. G. 1974, *MNRAS*, 166, 513
- Strom, K. M., Strom, S. E., Edwards, S., Cabrit, S., & Skrutskie, M. F. 1989, *AJ*, 97, 1451
- Taylor, G. 1960, *Proc. Roy. Soc. London, Series A*, 259, 1
- von Weizsäcker, C. F. 1943, *Zert. Astrophys.*, 22, 319

A. Capella: Instituto de Matemáticas, Universidad Nacional Autónoma de México, Área de la Inv. Científica, Circuito Exterior, Ciudad Universitaria, C.P. 04510, México, D.F., Mexico (capella@im.unam.mx).

X. Hernández: Instituto de Astronomía, Universidad Nacional Autónoma de México, Apdo. Postal 70-264, C.P. 04510, México, D.F., Mexico (xavier@astro.unam.mx).

Pablo L. Rendón and Rosa G. Rodríguez-Mota: Centro de Ciencias Aplicadas y Desarrollo Tecnológico, Universidad Nacional Autónoma de México, Apdo. Postal 70-186, C.P. 04510, México, D.F., Mexico (pablo.rendon@ccadet.unam.mx, rosa.g.asor@gmail.com).